Diffusion and Reaction in a Porous Catalyst Slab: Perturbation Solutions

Silvana S. S. Cardoso
Dept. of Chemical Engineering, Univ. of Cambridge, Pembroke Street, Cambridge CB2 3RA, U.K.

Alírio E. Rodrigues
LSRE, Departamento de Engenharia Química, Faculdade de Engenharia da Universidade do Porto, Rua Dr. Roberto Frias, 4200–465 Porto, Portugal

DOI 10.1002/aic.11009
Published online September 27, 2006 in Wiley InterScience (www.interscience.wiley.com).

The problem of diffusion and reaction in a porous catalyst slab is revisited. A combination of perturbation and integral mathematical techniques are used to derive approximate analytical solutions for the concentration and temperature profiles, as well as the effectiveness factor, for a first order, non-isothermal reaction. The development of thermal and concentration boundary layers near the surface of the particle is characterized. The internal particle resistances to mass and heat transfer are also calculated. Our analytical solutions are validated by comparison with previous numerical results. © 2006 American Institute of Chemical Engineers *AIChE J,* 52: 3924–3932, 2006
Keywords: diffusion and reaction, non-isothermal, porous catalyst, perturbation solutions

Introduction

Many chemical and biochemical reactions take place within porous catalyst particles. Most of these reactions have an appreciable heat of reaction. As a result, the interaction between heat conduction, diffusion of reactants and products, and chemical reaction has an important role in the performance of the catalyst. Such interaction has been studied extensively for the past 50 years and, in his treatise entitled *The Mathematical Theory of Diffusion and Reaction in Permeable Catalysts*, Rutherford Aris[1] presented a comprehensive review of the literature up to 1975. Since then, a number of other scientific publications have considered either new mathematical approaches or added complexity, such as biological kinetic schemes and transport by convection, in addition to diffusion, inside the catalyst particle.[2-5]

A description of the interaction between diffusion and chemical reaction within a porous catalyst particle involves analyzing and/or solving the differential equations for conservation of energy and mass of chemical species. For the case of a non-isothermal system, these equations are coupled and highly non-linear owing to the Arrhenius exponential dependence of the reaction rate on temperature. As a result, the problem is difficult to solve analytically and, in general, requires a numerical approach.

The non-isothermal problem was first analyzed by Damkholer[6] and Prater,[7] who derived an analytical equation relating the temperature difference between the center and the boundary of a porous particle to the reactant concentration difference. This relation allows an estimation of an upper bound for the maximum temperature inside a catalyst particle, and is independent of the kinetics of reaction and of particle geometry.

The problem was subsequently approached numerically by, among others, Carberry,[8] who examined first and second order kinetics in a catalyst of slab geometry, and Weisz and Hicks,[9] who considered first order kinetics in a spherical catalyst particle. Both these studies presented results for the effectiveness factor as a function of the Thiele modulus. Marek and Hlavacek[10] extended these studies and calculated the effectiveness factor for a broad selection of Prater and Arrhenius numbers, for first and second order kinetics, in slab, cylindrical, and spherical particle geometries.

Correspondence concerning this article should be addressed to S. S. S. Cardoso at SSSC1@cam.ac.uk.

Despite the mathematical complexity of the non-isothermal problem, significant progress has been made analytically. Tinkler and Pigford[11] conducted a perturbation analysis for a first order reaction in a sphere. They selected as small parameter a group involving the heat of reaction. Only results for the effectiveness factor versus Thiele modulus were presented, although at an intermediate stage the concentration and temperature profiles were also calculated. Hlavacek and Marek[12] derived approximate analytical expressions for the temperature profile and the effectiveness factor for a zeroth order reaction in catalyst particles of slab and cylindrical geometry. Their solution required an approximation to the exponential dependence of reaction rate on temperature. Drott and Aris[13] were the first to provide an analytical parametric solution for first order kinetics in a slab. Solving the problem by quadratures, they obtained analytical expressions for the concentration and temperature profiles in terms of exponential integrals. A general solution for the effectiveness factor was also provided. However, these solutions are all implicit and difficult to use.

Drott and Aris did analyze the behavior of their solutions in the limits of small and large Thiele modulus. For small Thiele modulus, they obtained explicit relations for both the maximum temperature and the effectiveness factor, as functions of Thiele modulus. For large Thiele modulus, implicit integral expressions were obtained for the maximum temperature and the effectiveness factor. More recently, Tavera[14] was able to derive an exact analytical solution for the effectiveness factor for an n-th order reaction in a catalyst slab. This solution becomes fairly simple for low values of the Prater number.

In the present article, we use a combination of perturbation and integral mathematical techniques to derive approximate analytical solutions for the concentration and temperature profiles, as well as the effectiveness factor, for a first order, non-isothermal reaction occurring in a catalyst slab. The development of thermal and concentration boundary layers near the surface of the particle is characterized. The internal particle resistances to mass and heat transfer are also calculated.

Theory

Mass and energy balances

Consider a porous catalyst slab in which a first order chemical reaction A $\rightarrow$ B occurs, together with diffusion of heat and mass. The reaction is non-isothermal and irreversible. The two sides of the slab are maintained at uniform temperature and concentration of A, as shown in Figure 1. The transverse position within the slab is denoted by $\hat{x}$. The slab thickness, $2L$, is much smaller than its other dimensions, so that changes in temperature and concentration occur primarily in the $\hat{x}$-direction. Differential balances for mass of reactant A and energy are given, respectively, by:

$$0 = D\frac{d^2\hat{c}}{d\hat{x}^2} - k\hat{c} \tag{1}$$

$$0 = \kappa\frac{d^2\hat{T}}{d\hat{x}^2} + \frac{qk}{\rho C_p}\hat{c} \tag{2}$$

with boundary conditions

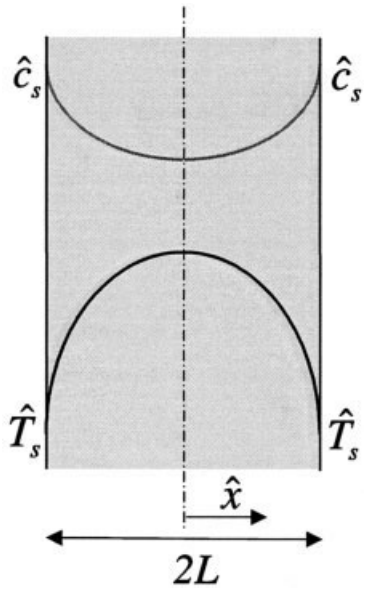

Figure 1. Catalyst slab, showing the profiles of concentration of reactant A (gray curve) and of temperature (black curve) for an exothermic reaction.

$$\hat{c} = \hat{c}_s \quad \text{and} \quad \hat{T} = \hat{T}_s \quad \text{at} \quad \hat{x} = \pm L \tag{3a, b}$$

Here, $\hat{c}$ denotes the concentration of reactant A, $\hat{T}$ is temperature, and the subscript s refers to surface conditions; k is the intrinsic kinetic constant, and D is the effective coefficient of diffusion of A within the porous matrix of the catalyst. The density, specific heat, and effective thermal diffusivity of the catalyst matrix filled with fluid are, respectively, ρ, C_p, and κ. The heat of reaction is q. In order to non-dimensionalize Eqs. 1 and 2, we define dimensionless concentration, temperature, and spatial position as follows:

$$c = \frac{\hat{c} - \hat{c}_s}{\hat{c}_s}, \quad T = \frac{\hat{T} - \hat{T}_s}{\Delta\hat{T}}, \quad x = \frac{\hat{x}}{L}, \tag{4a–c}$$

where $\Delta\hat{T}$ is a scale for the temperature change and is unknown at this stage.

The Arrhenius temperature dependence of the rate constant k can be expressed in non-dimensional form as:

$$k = k_0\exp\left(-\frac{E}{R\hat{T}}\right) = k_s\exp\left(\varphi\frac{T}{1+\eta T}\right) \tag{5}$$

Here, k_0 is a pre-exponential factor, k_s is the rate constant evaluated at the surface temperature of the catalyst,

$$\varphi = \frac{E\Delta\hat{T}}{R\hat{T}_s^2} \quad \text{and} \quad \eta = \frac{\Delta\hat{T}}{\hat{T}_s}. \tag{6a, b}$$

Substituting Eqs. 4 and 5 into Eqs. 1-3 leads to the non-dimensional mass and energy balances:

$$0 = \frac{d^2c}{dx^2} - \frac{k_sL^2}{D}\exp\left(\varphi\frac{T}{1+\eta T}\right)(c+1) \tag{7}$$

$$0 = \frac{d^2T}{dx^2} + \frac{q\hat{c}_s}{\rho C_p(\Delta\hat{T})}\frac{k_sL^2}{\kappa}\exp\left(\varphi\frac{T}{1+\eta T}\right)(c+1), \tag{8}$$

with boundary conditions

$$c = 0 \quad \text{and} \quad T = 0 \quad \text{at} \quad x = \pm 1. \tag{9a, b}$$

Scaling

Before we conduct a perturbation analysis, it is convenient to choose an appropriate scale for the temperature change in Eq. 4b. Given that the derivative term and the exponential factor in Eq. 8 should be of order unity, a balance of the heat conduction and reaction terms suggests that

$$\frac{q\hat{c}_s}{\rho C_p(\Delta\hat{T})}\frac{k_sL^2}{\kappa} \sim 1,$$

The expected temperature rise is, therefore,

$$(\Delta\hat{T}) \sim \frac{q\hat{c}_s}{\rho C_p}\frac{k_sL^2}{\kappa} = (\Delta\hat{T})_{ad}\frac{D}{\kappa}\phi^2, \tag{10}$$

where the Thiele modulus is

$$\phi = \left(\frac{k_sL^2}{D}\right)^{1/2} \tag{11}$$

and

$$(\Delta\hat{T})_{ad} = \frac{q\hat{c}_s}{\rho C_p} \tag{12}$$

is the adiabatic temperature change, which would occur after complete reaction if the concentration of reactant inside the catalyst were initially $\hat{c}_s$ at all positions and there were no heat loss/gain at the surface of the slab. As one might have intuitively anticipated, Eq. 10 shows that the temperature change inside the catalyst decreases with the thermal diffusivity and increases with the square of the thickness of the slab, that is, is directly proportional to time scale for heat conduction through the slab. In fact, Eq. 10 simply states that the time scale for heat generation/depletion by reaction is of the same order as the time scale for heat conduction across the slab.

Perturbation analysis

The scaling in the previous section suggests that we choose the adiabatic temperature change $(\Delta\hat{T})_{ad}$ as the scale for temperature change in the non-dimensionalization in Eq. 4. In this way, the Thiele modulus appears explicitly and may be used as the small or large parameter in a perturbation analysis. The governing equations then become:

$$0 = \frac{d^2c}{dx^2} - \phi^2\exp\left(\varphi\frac{T}{1+\eta T}\right)(c+1) \tag{13}$$

$$0 = \frac{d^2T}{dx^2} + \phi^2\frac{D}{\kappa}\exp\left(\varphi\frac{T}{1+\eta T}\right)(c+1) \tag{14}$$

with boundary conditions

$$c = 0 \quad \text{and} \quad T = 0 \quad \text{at} \quad x = \pm 1. \tag{15a, b}$$

We now conduct a perturbation analysis (see, for example, Bender and Orszag[15]) and look for solutions of Eqs. 13-15 of the form

$$c(x) = \sum_{n=0}^{\infty} c_n(x)\varepsilon^n \tag{16}$$

$$T(x) = \sum_{n=0}^{\infty} T_n(x)\varepsilon^n \tag{17}$$

where ε is a small parameter, and $c_n(x)$ and $T_n(x)$ are perturbation functions of order n. Substituting Eqs. 16 and 17 into Eqs. 13 and 14 yields:

$$0 = \frac{d^2}{dx^2}[c_0 + c_1\varepsilon + c_2\varepsilon^2 + O(\varepsilon^3)] - \phi^2\exp\left\{\varphi\frac{T_0 + T_1\varepsilon + T_2\varepsilon^2 + O(\varepsilon^3)}{1+\eta[T_0 + T_1\varepsilon + T_2\varepsilon^2 + O(\varepsilon^3)]}\right\} \times [1 + c_0 + c_1\varepsilon + c_2\varepsilon^2 + O(\varepsilon^3)] \tag{18}$$

$$0 = \frac{d^2}{dx^2}[T_0 + T_1\varepsilon + T_2\varepsilon^2 + O(\varepsilon^3)] + \phi^2\frac{D}{\kappa}\exp\left\{\varphi\frac{T_0 + T_1\varepsilon + T_2\varepsilon^2 + O(\varepsilon^3)}{1+\eta[T_0 + T_1\varepsilon + T_2\varepsilon^2 + O(\varepsilon^3)]}\right\} \times [1 + c_0 + c_1\varepsilon + c_2\varepsilon^2 + O(\varepsilon^3)] \tag{19}$$

The boundary conditions are expanded in a similar manner to give:

$$\begin{aligned} c_0 + c_1\varepsilon + c_2\varepsilon^2 + O(\varepsilon^3) &= 0 \\ T_0 + T_1\varepsilon + T_2\varepsilon^2 + O(\varepsilon^3) &= 0 \end{aligned} \quad \text{at} \quad x = \pm 1 \tag{20a, b}$$

Behavior for small Thiele modulus

When the Thiele modulus is small ($\phi^2 \ll 1$), chemical reaction is but a perturbation in a catalyst slab with simultaneous diffusion of heat and mass. In this limit, we make $\varepsilon = \phi^2 \ll 1$ in Eqs. 18-20 When the coefficients of successive powers of ε are separately equated to zero, an infinite set of differential equations and a sufficient set of boundary conditions are obtained.

The $O(1)$ problem is the same as setting $\varepsilon = 0$ in the original

equations, that is, a diffusive system with no reaction, and has solution:

$$c_0 = 0$$
$$T_0 = 0 \qquad (21a, b)$$

The $O(\varepsilon)$ problem yields the perturbation functions:

$$c_1 = \frac{1}{2}(x^2 - 1)$$
$$T_1 = -\frac{1}{2}\frac{D}{\kappa}(x^2 - 1) \qquad (22a, b)$$

At $O(\varepsilon^2)$, the solutions are:

$$c_2 = \frac{1}{24}\left(1 - \frac{D}{\kappa}\varphi\right)(5 - 6x^2 + x^4)$$
$$T_2 = -\frac{1}{24}\frac{D}{\kappa}\left(1 - \frac{D}{\kappa}\varphi\right)(5 - 6x^2 + x^4) \qquad (23a, b)$$

Thus, the first three terms of the expansions for $c(x)$ and $T(x)$ are

$$c(x) = \phi^2\frac{1}{2}(x^2 - 1) + \phi^4\frac{1}{24}\left(1 - \frac{D}{\kappa}\varphi\right) \times (5 - 6x^2 + x^4) + O(\phi^6)$$
$$T(x) = -\phi^2\frac{1}{2}\frac{D}{\kappa}(x^2 - 1) - \phi^4\frac{1}{24}\frac{D}{\kappa}\left(1 - \frac{D}{\kappa}\varphi\right) \times (5 - 6x^2 + x^4) + O(\phi^6) \qquad (24a, b)$$

For an exothermic reaction, the maximum temperature and the minimum concentration occur at $x = 0$ and are given by, respectively,

$$c_{\min} = c(0) = -\frac{\phi^2}{2} + \phi^4\frac{5}{24}\left(1 - \frac{D}{\kappa}\varphi\right) + O(\phi^6)$$
$$T_{\max} = T(0) = \frac{\phi^2}{2}\frac{D}{\kappa} - \phi^4\frac{5}{24}\frac{D}{\kappa}\left(1 - \frac{D}{\kappa}\varphi\right) + O(\phi^6) \qquad (25a, b)$$

Behavior for large Thiele modulus

When the Thiele modulus is large ($\phi^2 \gg 1$), the chemical reaction is fast and leads to a sharp decline in concentration near the surface of the catalyst slab. Similarly, there is a sharp change in temperature near the edges of the slab: an increase for exothermic and a decrease for endothermic reactions. Thus, concentration and thermal boundary layers develop at $\hat{x} = \pm L$, as shown in Figure 2. In this limit, we conduct a singular perturbation analysis and look for solutions of Eqs. 18-20 but now with $\varepsilon = 1/\phi^2 \ll 1$ as the small parameter.

Middle Region. In the region of the catalyst slab away from the boundary layers, that is, in the middle region (Figure 2), Eqs. 18-20 hold and we can simply collect terms of similar order with respect to the small parameter $\varepsilon = 1/\phi^2$. We denote the concentration and temperature in this region by $c^m(x)$ and $T^m(x)$, respectively. Solution of the $O(1)$ problem gives:

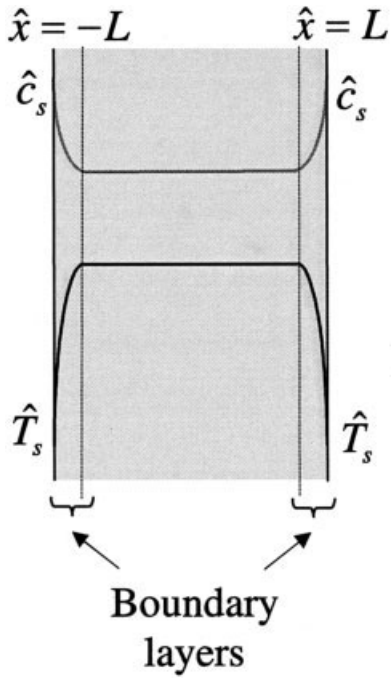

Figure 2. Catalyst slab, showing the concentration and thermal boundary layers that develop for $\phi^2 \gg 1$.

$$c_0^m = -1 \qquad (26)$$

and no information is gained about $T_0^m(x)$. At $O(\varepsilon)$, we find:

$$c_1^m = 0$$
$$T_0^m = ax + d \qquad (27a, b)$$

where a and d are constants to be determined.

Region Near $x = 1$. In the boundary layer near $x = 1$, the stretching transformation

$$X = (1 - x)\varepsilon^{-1/2} \qquad (28)$$

is applied. Using Eq. 25 in the mass and energy balances Eqs. 13-15, yields:

$$0 = \frac{d^2c^{rb}}{dX^2} - \exp\left(\varphi\frac{T^{rb}}{1 + \eta T^{rb}}\right)(c^{rb} + 1) \qquad (29)$$

$$0 = \frac{d^2T^{rb}}{dX^2} + \frac{D}{\kappa}\exp\left(\varphi\frac{T^{rb}}{1 + \eta T^{rb}}\right)(c^{rb} + 1) \qquad (30)$$

with boundary conditions

$$c^{rb} = 0 \quad \text{and} \quad T^{rb} = 0 \quad \text{at} \quad X = 0 \qquad (31a, b)$$

where $c^{rb}(X)$ and $T^{rb}(X)$ refer to the concentration and temperature in the right-hand-side boundary layer. After expansion of $c^{rb}(X)$ and $T^{rb}(X)$ in power series in $\varepsilon = 1/\phi^2$ and collection of terms of $O(1)$ in Eqs. 29 and 30, we obtain:

$$c_0^{rb} = -\frac{\kappa}{D} T_0^b \tag{32}$$

$$0 = \frac{d^2 T_0^{rb}}{dX^2} + \left(\frac{D}{\kappa} - T_0^{rb}\right) \exp\left(\varphi \frac{T_0^b}{1 + \eta T_0^{rb}}\right) \tag{33}$$

Equation 33 is non-linear and cannot be solved analytically in an exact manner. However, we may find an approximate solution. Matching the middle and right boundary layer solutions, we have:

$$\lim_{X \to \infty} c_0^{rb} = \lim_{x \to 1} c_0^m = -1, \quad \varepsilon \to 0 \tag{34}$$

and

$$\lim_{X \to \infty} T_0^{rb} = \lim_{x \to 1} T_0^m = \frac{D}{\kappa}, \quad \varepsilon \to 0 \tag{35}$$

We, therefore, expect that:

$$c_0^{rb} = -1 + w(X)$$

$$T_0^{rb} = \frac{D}{\kappa}[1 - w(X)] \tag{36a, b}$$

where $\lim_{X \to \infty} w(X) = 0$. From the boundary conditions, Eq. 31, we also have $\lim_{X \to 0} w(X) = 1$. Substituting Eq. 36b into Eq. 33 yields:

$$0 = \frac{d^2 w}{dX^2} - w \exp\left(\varphi \frac{D}{\kappa} \frac{1 - w}{1 + \eta \frac{D}{\kappa} 1 - w}\right) \tag{37}$$

For small $\varphi D/\kappa$ and $\eta D/\kappa$, we may make the simplification:

$$\exp\left(\varphi \frac{D}{\kappa} \frac{1 - w}{1 + \eta \frac{D}{\kappa} 1 - w}\right) \approx b^2 \tag{38}$$

and treat b as approximately constant. Then $w(X) \approx e^{-bX}$.

Substituting this result into Eqs. 36 gives:

$$c_0^{rb} = -1 + e^{-bX}$$

$$T_0^{rb} = \frac{D}{\kappa}[1 - e^{-bX}] \tag{39a, b}$$

In order to determine b, we force the energy balance (Eq. 33) to be satisfied integrally in the whole of the boundary layer:

$$0 = \int_0^\infty \left[\frac{d^2 T_0^{rb}}{dX^2} + \left(\frac{D}{\kappa} - T_0^{rb}\right) \exp\left(\varphi \frac{T_0^b}{1 + \eta T_0^{rb}}\right)\right] dX \tag{40}$$

For small $\eta D/\kappa$, Eq. 40 has solution:

$$b = \left(\frac{e^{\varphi D/\kappa} - 1}{\varphi D/\kappa}\right)^{1/2} \tag{41}$$

Region Near $x = -1$. In the left-hand-side boundary layer, near $x = -1$, we apply the stretching transformation

$$Y = (1 + x)\varepsilon^{-1/2} \tag{42}$$

We may follow a solution procedure similar to that for the right boundary layer and substitute this transformation into the balances (Eqs. 13-15). However, it is simpler to notice that the behavior of the catalyst slab is symmetrical with respect to $x = 0$, so we expect solutions

$$c_0^{lb} = -1 + be^{-Y}$$

$$T_0^{lb} = \frac{D}{\kappa}[1 - be^{-Y}] \tag{43a, b}$$

in the left boundary layer.

Composite Solution. The final composite solution, valid across the whole of the catalyst width, is given by:

$$c = c^{lb} + c^m + c^{rb} - \lim_{Y \to \infty} c^{lb} - \lim_{X \to \infty} c^{rb}$$

$$T = T^{lb} + T^m + T^{rb} - \lim_{Y \to \infty} T^{lb} - \lim_{X \to \infty} T^{rb} \tag{44a, b}$$

From Eqs. 27b and 35 and symmetry considerations, we deduce that $a = 0$ and $d = D/\kappa$, so that $T_0^m = D/\kappa$.

Equations 44 then yield:

$$c(x) = -1 + e^{-b(1-x)\phi} + e^{-b(1+x)\phi} + O(\phi^{-2})$$

$$T(x) = \frac{D}{\kappa}[1 - e^{-b(1-x)\phi} - e^{-b(1+x)\phi}] + O(\phi^{-2}) \tag{45a, b}$$

We conclude that for large Thiele modulus, the minimum concentration and maximum temperature for an exothermic reaction are:

$$c_{\min} = c(0) = -1 + O(\phi^{-2})$$
$$T_{\max} = T(0) = \frac{D}{\kappa} + O(\phi^{-2}) \tag{46a, b}$$

The effectiveness factor

The overall performance of a catalyst slab is measured by its effectiveness factor,

Table 1. Perturbation Solutions for the Effectiveness Factor, Maximum Temperature, and Concentration of Reactant and Temperature Profiles Inside a Catalyst Slab for a First Order Chemical Reaction

	$\phi^2 \ll 1$	$\phi^2 \gg 1$	
Effectiveness factor, *Eff*	$1 - \frac{\phi^2}{3}(1 - \gamma\beta)$	$\frac{b}{\phi}[1 - \exp(-2b\phi)]$	(54a, b)
Maximum temperature, $\hat{T}_{\max}/\hat{T}_s$	$1 + \beta\frac{\phi^2}{2} - 5\beta\frac{\phi^4}{24}(1 - \gamma\beta)$	$1 + \beta$	(55a, b)
Concentration profile, $\hat{c}/\hat{c}_s$	$1 - \frac{\phi^2}{2}(1 - x^2) + \frac{\phi^4}{24}(1 - \gamma\beta)(5 - 6x^2 + x^4)$	$\exp[-b(1 - x)\phi] + \exp[-b(1 + x)\phi]$	(56a, b)
Temperature profile, $\hat{T}/\hat{T}_s$	$1 + \beta\left\{\frac{\phi^2}{2}(1 - x^2) - \frac{\phi^4}{24}(1 - \gamma\beta)(5 - 6x^2 + x^4)\right\}$	$1 + \beta\{1 - \exp[-b(1 - x)\phi] - \exp[-b(1 + x)\phi]\}$	(57a, b)
		where $b = \left(\frac{e^{\gamma\beta} - 1}{\gamma\beta}\right)^{1/2}$	(58)

$$Eff = \frac{\int_{-L}^{+L} k\hat{c}\,d\hat{x}}{\int_{-L}^{+L} k_s\hat{c}_s\,d\hat{x}}, \tag{47}$$

which compares the average reaction rate to the reaction rate that would be observed if the concentration of reactant and temperature throughout the slab were equal to those at the surface. Using Gauss's divergence theorem, it may be shown that in terms of our non-dimensional variables,

$$Eff = \frac{1}{2\phi^2}\left(\left.\frac{dc}{dx}\right|_{x=1} - \left.\frac{dc}{dx}\right|_{x=-1}\right) \tag{48}$$

It is now very easy to determine the effectiveness factor in the limits of small and large Thiele modulus. Using our results Eqs. 24 and 45 in Eq. 47 gives:

$$Eff = 1 - \frac{\phi^2}{3}\left(1 - \frac{D}{\kappa}\varphi\right) + O(\phi^4) \quad \text{for} \quad \phi^2 \ll 1$$

$$Eff = \frac{b}{\phi}(1 - e^{-2b\phi}) + O(\phi^{-4}) \quad \text{for } \phi^2 \gg 1 \tag{49a, b}$$

Particle internal resistances to mass and heat transfer

It may be of interest to have expressions for the intraparticle resistance to heat and mass transfer. Hence, we may define the internal resistance to mass transfer, R_{mi}, by

$$-D\left.\frac{d\hat{c}}{d\hat{x}}\right|_{\hat{x}=L} = \frac{1}{R_{mi}}(\hat{c}_{\min} - \hat{c}_s) \tag{50}$$

Similarly, the internal resistance to heat transfer, R_{hi}, is defined by

$$-\kappa\rho C_p\left.\frac{d\hat{T}}{d\hat{x}}\right|_{\hat{x}=L} = \frac{1}{R_{hi}}(\hat{T}_{\max} - \hat{T}_s), \tag{51}$$

Using results Eq. 24 in the expressions above, we have for $\phi^2 \ll 1$,

$$\frac{1}{R_{mi}} = \frac{2D}{L}\frac{1 - \frac{\phi^2}{3}\left(1 - \frac{\varphi D}{\kappa}\right)}{1 - \frac{5}{12}\phi^2\left(1 - \frac{\varphi D}{\kappa}\right)}$$

$$\frac{1}{R_{hi}} = \frac{2\kappa\rho C_p}{L}\frac{1 - \frac{\phi^2}{3}\left(1 - \frac{\varphi D}{\kappa}\right)}{1 - \frac{5}{12}\phi^2\left(1 - \frac{\varphi D}{\kappa}\right)}$$

For $\phi^2 \gg 1$, using results Eq. 45 in Eqs. 50 and 51, we find:

$$\frac{1}{R_{mi}} = \frac{D}{L}b\phi$$

$$\frac{1}{R_{hi}} = \frac{\kappa\rho C_p}{L}b\phi \tag{53a, b}$$

Discussion

The analytical solutions derived in the previous section allow the determination of the concentration and temperature profiles, as well as the effectiveness factor and transport rates, for a variety of operating conditions and particle characteristics. In this section, the behavior of our solutions in the isothermal limit is examined and a comparison with previous numerical data is presented.

The main results of the previous section may be expressed in terms of the well-known Prater $\beta = q\hat{c}_s D/(\rho C_p \hat{T}_s \kappa)$ and Arrhenius $\gamma = E/(R\hat{T}_s)$ numbers. Indeed, we note that $\varphi D/\kappa = \gamma\beta$ and $\eta D/\kappa = \beta$. Table 1 summarizes our results for the concentration and temperature profiles, as well as the effectiveness factor, in terms of β and γ.

We begin by looking at the behavior of our solutions in the isothermal limit, that is, when $\beta \to 0$. We note that in this case $b \to 1$ (see Eq. 58). Our results suggest that in this limit the temperature inside the slab is uniform and the concentration profile reduces to:

$$c = \frac{\phi^2}{2}(-1 + x^2) + \frac{\phi^4}{24}(5 - 6x^2 + x^4) \quad \text{for } \phi^2 \ll 1$$

$$c = -1 + \exp[-(1-x)\phi] + \exp[-(1+x)\phi] \quad \text{for } \phi^2 \gg 1 \tag{59a, b}$$

The effectiveness factor in this limit is given by:

$$Eff = 1 - \frac{\phi^2}{3} \quad \text{for } \phi^2 \ll 1$$

$$Eff = \frac{1}{\phi}[1 - \exp(-2\phi)] \approx \frac{1}{\phi} \quad \text{for } \phi^2 \gg 1 \tag{60a, b}$$

The relations in Eqs. 59 and 60 agree with previously published, well known results for an isothermal slab.[1]

Damkholer[6] and Prater[7] suggested that the maximum temperature inside a catalyst slab can be calculated from $\hat{T}_{max}/\hat{T}_s = 1 + \beta$ for an irreversible reaction. Their derivations required the assumption that the concentration at the center of the particle is zero. As we have seen (Table 1), this is only the case when the Thiele modulus is sufficiently large, in particular, $\phi^2 \gg 1$.

As mentioned in the introduction, Drott and Aris[13] obtained analytical expressions for the concentration and temperature profiles, as well as the effectiveness factor, in terms of exponential integrals. They analyzed the behavior of their solutions in the limits of small and large Thiele modulus. For $\phi \to 0$, they obtained explicit relations for both the effectiveness factor and the maximum temperature, as functions of Thiele modulus; our perturbation solutions (Eqs. 54a and 55a in Table 1) agree with their results. For $\phi \to \infty$, those authors obtained implicit integral expressions for the maximum temperature and the effectiveness factor; it is difficult to compare their results directly with our explicit perturbation solutions.

It is worth noting that for a zeroth order reaction, using Frank Kamenetskii's exponential approximation to the Arrhenius dependence of the reaction rate constant on temperature, Aris[1] showed that for large ϕ the effectiveness factor of a slab is given by $Eff = \sqrt{2}b/\phi$. This result is very similar to our solution (Eq. 54b) for a first order reaction, essentially just differing by a factor of $\sqrt{2}$. Such a similarity is not totally surprising given that, in the isothermal and large ϕ limit, it is well known that $Eff = [2/(n+1)]^{1/2}/\phi$ (see Aris[1]).

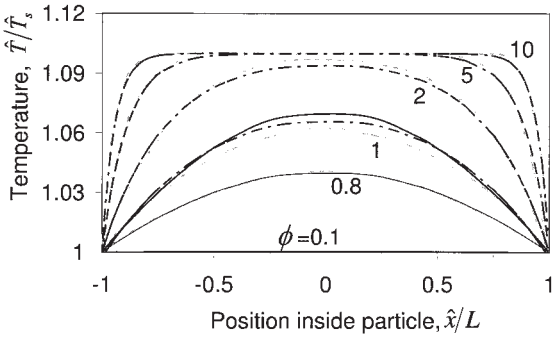

Figure 4. Temperature profile inside a catalyst slab for a first-order chemical reaction.

Shown are the numerical results of Quinta Ferreira (gray lines),[16] the regular perturbation predictions for low Thiele modulus (solid black lines), and the singular perturbation predictions for high Thiele modulus (dashed black lines), for $\gamma = 20$ and $\beta = 0.1$.

In order to test directly the accuracy of our approximate perturbation solutions, we compare their predictions with the results obtained from numerical integration of the governing equations. As mentioned in the introduction, many previous studies have presented numerical results on the behavior of a catalyst slab undergoing a first order, non-isothermal reaction. Here, we shall use the results reported by Marek and Hlavacek[10] and Quinta Ferreira,[16] because these were readily available in a convenient format. Figures 3 and 4 show a comparison between the numerical results of Quinta Ferreira[16] and our analytical predictions for the concentration and temperature profiles. The agreement is very good. For low Thiele modulus, our regular perturbation solutions overlap with the numerical results. For large Thiele modulus, our singular perturbation predictions are close to the numerical solution; we recall that our results here involved an approximate solution of a nonlinear perturbation problem at $O(1)$, so the agreement is rather good. Figure 5 shows a comparison between the numerical results of Quinta Ferreira[16] and our analytical predictions for the maximum temperature. Again, we see an excellent agree-

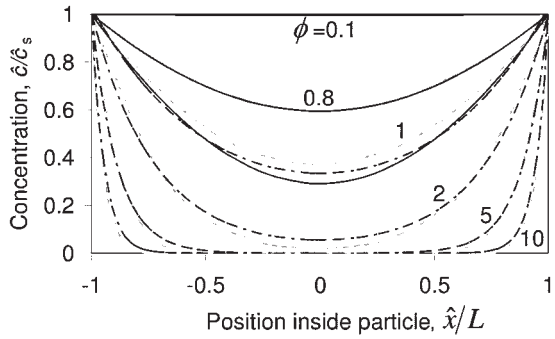

Figure 3. Reactant concentration profile inside a catalyst slab for a first-order chemical reaction.

Shown are the numerical results of Quinta Ferreira (gray lines),[16] the regular perturbation predictions for low Thiele modulus (solid black lines), and the singular perturbation predictions for high Thiele modulus (dashed black lines), for $\gamma = 20$ and $\beta = 0.1$.

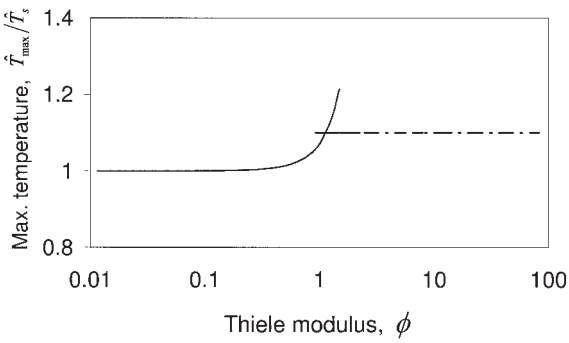

Figure 5. Maximum temperature inside a catalyst slab for a first-order chemical reaction.

Shown are the numerical results of Quinta Ferreira (gray line),[16] the regular perturbation predictions for low Thiele modulus (solid black line), and the singular perturbation predictions for high Thiele modulus (dashed black line), for $\gamma = 20$ and $\beta = 0.1$.

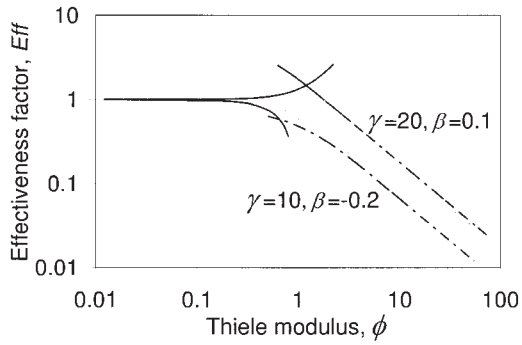

Figure 6. Effectiveness factor of a catalyst slab for a first-order chemical reaction.

Shown are the numerical results of Quinta Ferreira (gray line for $\gamma = 20$ and $\beta = 0.1$)[16] and Marek and Hlavacek (gray line for $\gamma = 10$ and $\beta = -0.2$),[10] as well as the corresponding regular perturbation predictions for low Thiele modulus (solid black lines) and singular perturbation predictions for high Thiele modulus (dashed black lines).

ment for low Thiele modulus and a good analytical prediction for high Thiele modulus.

The dependence of the effectiveness factor on the Thiele modulus is shown in Figure 6. The numerical and approximate analytical results are in very good agreement for a selection of Arrhenius and Prater numbers. In general, for small β and $|\gamma\beta| < 2$, the agreement between the theoretical and numerical results for large ϕ is good. As $|\gamma\beta|$ is increased, the deviation between the theory and the numerics increases; the effectiveness factor is overestimated by the theory for $\beta > 0$ and underestimated for $\beta < 0$. Once more, we note that this deviation is not surprising given that, when solving Eq. 37, we assumed both β and $\varphi D/\kappa = \gamma\beta$ to be small.

The stretching transformation in Eq. 28 and results Eq. 49 show that, for large ϕ, the concentration and thermal boundary layers at the surface of the slab have equal thickness $\ell = O(L\varepsilon^{1/2}) = O(L\phi^{-1}) = O[(D/k_s)^{1/2}]$. Thus, the thickness of the concentration and thermal boundary layers is proportional to the square root of the coefficient of diffusion of reactant A within the porous catalyst particle multiplied by the timescale for chemical reaction. This conclusion is in accord with the fact that the particle internal resistances to mass and heat transfer predicted in Eqs. 53a and b are inversely proportional to the Thiele modulus.

As a final note, we recall that in this work we have assumed the concentration and temperature at the surface of the catalyst slab to be known and fixed at $\hat{c}_s$ and $\hat{T}_s$, respectively. This presumes the external resistances to mass and heat transfer to/from the slab to be negligible. However, the findings in this article also have relevance for situations in which these external resistances are significant. In such cases, only the concentration and temperature in the fluid at some distance from the slab will be known, respectively, $\hat{c}_\infty$ and $\hat{T}_\infty$; but the surface concentration and temperature are related to these through

$$-D\left.\frac{d\hat{c}}{d\hat{x}}\right|_{\hat{x}=L} = \frac{1}{R_{mi}}(\hat{c}_{\min} - \hat{c}_s) = k_m(\hat{c}_s - \hat{c}_\infty) \qquad (61)$$

$$-\kappa\rho C_p\left.\frac{d\hat{T}}{d\hat{x}}\right|_{\hat{x}=L} = \frac{1}{R_{hi}}(\hat{T}_{\max} - \hat{T}_s) = h(\hat{T}_s - \hat{T}_\infty), \qquad (62)$$

where k_m and h are the external mass transfer and heat transfer coefficients, respectively. Therefore, in order to calculate the concentration and temperature profiles inside the catalyst slab in the presence of external surface resistances, one needs an iterative procedure. One should start by guessing values for $\hat{c}_s$ and $\hat{T}_s$ (a good initial estimate is setting $\hat{c}_s = \hat{c}_\infty$ and $\hat{T}_s = \hat{T}_\infty$), then use the results in Table 1 to calculate the internal concentration and temperature profiles, and, finally, iterate estimating new values of $\hat{c}_s$ and $\hat{T}_s$ from Eqs. 61 and 62, respectively. The iteration should be repeated until the desired accuracy in $\hat{c}_s$ and $\hat{T}_s$ is achieved.

Conclusions

The interaction between heat conduction, diffusion of reactants and products, and chemical reaction within a porous catalyst particle of slab geometry has been analyzed. A combination of perturbation and integral mathematical techniques was used to derive approximate analytical solutions for the concentration and temperature profiles, as well as the effectiveness factor, for a first order, non-isothermal reaction. It was shown that for large Thiele modulus, thermal and concentration boundary layers develop near the surface of the particle; these boundary layers have thickness proportional to the square root of the coefficient of diffusion of reactant within the porous catalyst particle multiplied by the timescale for chemical reaction. Expressions were developed for the internal particle resistances to mass and heat transfer. Our analytical solutions were validated by comparison with previous numerical results. It was shown that there is good agreement between theory and numerics for small β and $|\gamma\beta| < 2$, where β and γ are the Prater and Arrhenius numbers, respectively.

Acknowledgments

This work was conducted during the sabbatical leave of SSSC at the University of Porto. Travel funding from the EPSRC through grant EP/C547780/1 is gratefully acknowledged.

Notation

a = a constant
b = parameter defined Eq. 58
c = dimensionless concentration of reactant A
c_n = perturbation function of order n for dimensionless concentration
$\hat{c}$ = concentration of reactant A
$\hat{c}_s$ = concentration of reactant A at the surface of the slab
$\hat{c}_\infty$ = concentration of reactant A at some distance from the slab
C_p = specific heat of catalyst matrix filled with fluid
d = a constant
D = effective coefficient of diffusion of A within the porous matrix of the catalyst
E = activation energy for the reaction
Eff = effectiveness factor
k = intrinsic kinetic constant of the reaction
k_m = external mass transfer coefficient
k_s = kinetic rate constant evaluated at the surface temperature of the catalyst
k_0 = pre-exponential factor in the Arrhenius rate law
h = external heat transfer coefficient
L = semi-thickness of the slab
ℓ = thickness of the concentration and thermal boundary layers at the left and right surfaces of the slab
q = heat of reaction
R = universal gas constant
R_{hi} = internal resistance to heat transfer
R_{mi} = internal resistance to mass transfer

T = dimensionless temperature
T_n = perturbation function of order n for dimensionless temperature
$\hat{T}$ = temperature
$\hat{T}_s$ = temperature at the surface of the slab
$\hat{T}_\infty$ = temperature at some distance from the slab
$\Delta\hat{T}$ = scale for the temperature change
$(\Delta\hat{T})_{ad}$ = adiabatic temperature change
x = dimensionless transverse position within the slab
$\hat{x}$ = transverse position within the slab
X = stretched coordinate in the region near $x = 1$
Y = stretched coordinate in the region near $x = -1$
w = function defined in Eq. 36

Greek letters

$\beta = q\hat{c}_s D/(\rho C_p \hat{T}_s \kappa)$ = the Prater number
ε = small parameter in perturbation expansion
$\phi = (k_s L^2/D)^{1/2}$ = the Thiele modulus
φ = parameter defined in Eq. 6a
$\gamma = E/(R\hat{T}_s)$ = the Arrhenius number
η = parameter defined in Eq. 6b
κ = effective thermal diffusivity of catalyst matrix filled with fluid
ρ = density of catalyst matrix filled with fluid

Subscripts

max = maximum
min = minimum
n = 0, 1, 2, . . . the order of the perturbation function
s = surface of the slab

Superscripts

lb = left-hand-side boundary layer in the slab
m = middle region in the slab
rb = right-hand-side boundary layer in the slab

Literature Cited

1. Aris R. *The Mathematical Theory of Diffusion and Reaction in Permeable Catalysts: Vol. 1—The Theory of Steady State*. Oxford: Clarendon Press; 1975.
2. Nir A, Pismen L. Simultaneous intraparticle forced convection, diffusion and reaction in a porous catalyst. *Chem Eng Sci.* 1977;32:35-41.
3. Rodrigues AE, Orfão JM. Intraparticle convection, diffusion and zero order reaction in porous catalyst. *Chem Eng Commun.* 1984;27:327-337.
4. Stephanopoulos G, Tsiveriotis K. The effect of intraparticle convection on nutrient transport in porous biological pellets. *Chem Eng Sci.* 1989;44:2031-2039.
5. Lopes JCB, Dias MM, Mata VG, Rodrigues AE. Flow field and non-isothermal effects on diffusion, convection and reaction in permeable catalysts. *Ind Eng Chem Res.* 1995;34:148-157.
6. Damkholer G. The adsorption velocity of gases on porous adsorbents. *Zeitschrift für physikalische.* 1935;A174:228-238.
7. Prater CD. The temperature produced by heat of reaction in the interior of porous particles. *Chem Eng Sci.* 1958;8:284-286.
8. Carberry JJ. The catalytic effectiveness factor under nonisothermal conditions. *AIChE J.* 1961;87:350-357.
9. Weisz PB, Hicks JS. The behaviour of porous catalyst particles in view of internal mass and heat diffusion effects. *Chem Eng Sci.* 1962;17:265-275.
10. Marek M, Hlavacek V. Nonisothermal first and second order reaction within a porous catalyst particle. *Scientific Papers of the Institute of Chemical Tech Prague.* 1969;K3:19-45.
11. Tinkler JD, Pigford RL. The influence of heat generation on the catalyst effectiveness factor. *Chem Eng Sci.* 1961;15:326-328.
12. Hlavacek V, Marek M. Modelling of chemical reactors—IX: Nonisothermal zero-order reaction within a porous catalyst particle. *Chem Eng Sci.* 1968;23:865-880.
13. Drott DW, Aris R. Communications on the theory of diffusion and reaction—I. A complete parametric study of the first order, irreversible exothermic reaction on a slab of catalyst. *Chem Eng Sci.* 1969;24:541-551.
14. Tavera EM. Analytical expression for the non-isothermal effectiveness factor: the n-th order reaction in a slab geometry. *Chem Eng Sci.* 2005;60:907-916.
15. Bender CM, Orszag SA. *Advanced Mathematical Methods for Scientists and Engineers*. New York: Springer-Verlag; 1999.
16. Quinta Ferreira RM. Contribuição para o estudo de reactores catalíticos de leito fixo. Efeito da convecção em catalisadores de poros largos e casos de catalisadores bidispersos. PhD Thesis, University of Porto, 1988.

Manuscript received May 1, 2006, and revision received Aug. 11, 2006.